PAPER

Check for updates

Lithium isotope tracing in silicon-based electrodes using solid-state MAS NMR: a powerful comprehensive tool for the characterization of lithium batteries†

Manon Berthault,[a] Anton Buzlukov, [ID] *[bc] Lionel Dubois,[d] Pierre-Alain Bayle,[b] Willy Porcher,[a] Thibaut Gutel, [ID] [a] Eric De Vito [ID] [e] and Michel Bardet [ID] *[b]

The introduction of lithiated components with different $^7Li/^6Li$ isotopic ratios, also called isotopic tracing, can give access to better understanding of lithium transport and lithiation processes in lithium-ion batteries. In this work, we propose a simple methodology based on high-resolution solid-state NMR for the determination of the $^7Li/^6Li$ ratio in silicon electrodes following different strategies of isotopic tracing. The ^6Li and ^7Li MAS NMR experiments allow obtaining resolved spectra whose spectral components can be assigned to different moieties of the materials. In order to measure the ratio of the $^6Li/^7Li$ NMR integrals, a silicon electrode with a natural $^7Li/^6Li$ isotope abundance was used as a reference. This calibration can then be used to determine the $^7Li/^6Li$ ratio of any similar samples. This method was applied to study the phenomena occurring at the interface between a silicon electrode and a labeled electrolyte, which is an essential step for isotopic tracing experiments in systems after the formation of the solid electrolyte interphase (SEI). Beyond the isotopic exchanges between the SEI and the electrolyte already observed in the literature, our results show that isotopic exchanges also involve Li–Si alloys in the electrode bulk. Within a 52-hour contact, the electrolyte labeling disappeared: isotopic concentrations of the electrolyte and electrode become practically homogenized. However, at the electrode level, different silicides are characterized by rather different isotopic enrichment. In the present work, ToF SIMS and liquid state NMR were also used to cross-check and discuss the solid-state NMR method we have proposed.

1. Introduction

Experiments based on isotope tracing have already been successfully applied in a wide range of domains: biology, medicine, environmental sciences,[1] chemistry and physics. However, depending on the questions being addressed, they have not been developed and applied to the same extent. In the field of materials for energy storage, such an approach has been proposed to study Li-ion batteries, though it still remains at a very early stage. Since 2011, only a dozen publications have used it for studying the SEI structure,[2] SEI formation[3] and Li

[a] Univ. Grenoble Alpes, CEA, Liten, DEHT, 38000 Grenoble, France
[b] Univ. Grenoble Alpes, CEA, IRIG, MEM, 38000 Grenoble, France.
  E-mail: michel.bardet@cea.fr
[c] IMP UB RAS—M.N. Miheev Institute of Metal Physics of Ural Branch of Russian
  Academy of Sciences, 620137 Ekaterinburg, Russia. E-mail: buzlukov@mail.ru
[d] Univ. Grenoble Alpes, CEA, IRIG, SYMMES, 38000 Grenoble, France
[e] Univ. Grenoble Alpes, CEA, Liten, DTNM, 38000 Grenoble, France
† Electronic supplementary information (ESI) available. See DOI: https://doi.org/
10.1039/d3cp02646a

diffusion.[4–10] In this field, carbon and lithium nuclei are the favorite probes. As a matter of fact, lithium plays a crucial role in the operation of Li-ion batteries since it acts as a shuttle from one electrode to the other but it is also involved in many side reactions in various media at different states: the liquid phase of the electrolyte, the solid phase of electrode materials and the solid interphase between the negative electrode and the electrolyte (SEI).

During the first lithiation of the anode, part of the electrolyte is decomposed by reduction. Insoluble degradation products remain at the negative electrode surface and give rise to the SEI. The soluble counterpart remains in the electrolyte itself. A portion of lithium appears to be irreversibly trapped in the SEI associated with capacity fading. Carbon as a major element of the electrolyte is detected not only in the liquid phase but also in the SEI solid phase. It is also present in binder or conductive additives. Although it can be considered as a key element of Li-ion batteries, it remains a difficult probe compared with Li, especially for NMR due to its low sensitivity and the huge number of expected chemical shifts. However, carbon

This journal is © the Owner Societies 2023

Phys. Chem. Chem. Phys., 2023, **25**, 22145–22154 | **22145**

has been also used to study the dynamics of organic compounds in the electrolyte or in the SEI. ^{13}C NMR has shown that organic products observed in the SEI of silicon were mostly derived from ethylene carbonate (EC) rather than dimethylcarbonate (DMC) and that the degradation of EC with aging leads to the formation of linear alkylcarbonates-based oligomers with methoxide-end groups, accumulating in the electrolyte.[11] Using lithium tracing, the lithium diffusion coefficient in materials such as $LiMn_2O_4$, Li_3PO_4 or Li_xCoO_2[5,6,12,13] was determined and more general information regarding the lithium dynamics between the different phases of electrode materials was obtained.[14–18]

Irrespective of the technique used, a large part of the studies focuses on the interactions between the electrode and the electrolyte by monitoring their respective Li isotope contents in these two counterparts. In most of these experiments, an electrode is immersed in an electrolyte. Investigations on a model SEI using Time-of-Flight Secondary Ion Mass Spectrometry (ToF-SIMS) analysis have already shown that Li isotope exchanges take place quickly (~ 30 s) between the electrolyte and the SEI.[2] Similar isotope exchanges have been also observed on delithiated graphite electrodes *via* ToF-SIMS with the same types of experiments.[10] The results show that the diffusion of Li ions from the electrolyte to the SEI is very fast: the isotopic exchange is almost achieved in less than 20 min. From this, the thickness of the mineral part of the SEI has been estimated. However, while the Li isotope exchanges have been demonstrated between the electrolyte and SEI, no study has been realized considering Li in the active material. For instance, in the experiments carried out by Ilott *et al.*[15] and Gunnarsdóttir *et al.*,[17] they soaked a [6]Li metal piece in an electrolyte containing ^{7}Li and then monitored ^{7}Li NMR signals, corresponding to both the metal and the electrolyte during all the prolonged contact. In parallel, a numerical model has been developed to describe the process. It allowed them to quantify the growth of the SEI and the evolution of ion permeability into the Li metal. For isotopic tracing, the solid-state NMR is a promising tool since in addition to the quantitative analysis of each isotope, [7]Li and [6]Li, it provides information on their chemical environments. For instance, in a silicon-based electrode, the different silicides can be easily distinguished with solid-state [6,7]Li NMR.[19,20] This technique also enables to detect Li dendrites on graphite[21] and lithium metal electrodes.[22] Moreover, recent studies on either *in situ* NMR or *in situ* MRI raise a lot of expectations, especially to follow Li isotope exchange under *operando* conditions.[22] It is worthwhile to recall that NMR analyzes the whole sample, and some experimental conditions have to be fulfilled to provide quantitative data.

Concerning lithium at natural abundance, it has two isotopes [7]Li ($I = 3/2$) and [6]Li ($I = 1$) at 92.6% and 7.4%, respectively. On non-labelled compounds, the [7]Li and [6]Li fractions are expected to remain constant, while by introducing a [6]Li-enriched component during battery assembly, the evolution of the [7]Li/[6]Li ratio after battery cycling enables to identify various processes and trace lithium pathways. In principle, this
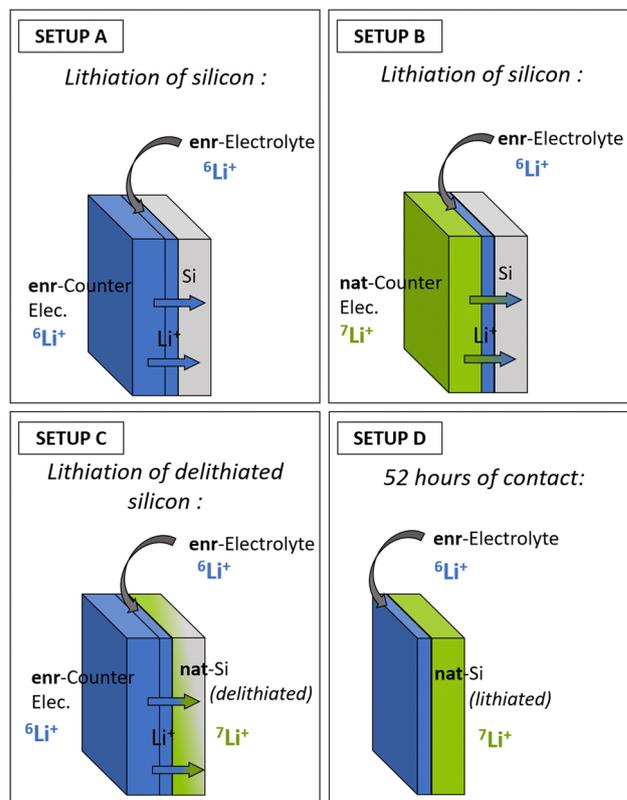

Fig. 1 [6]Li enrichment process for the four electrodes: (A–D) "Nat" and "enr" are used to characterize respectively "natural" and "enriched" components in [6]Li. In a nat-component, the lithium isotopic ratio is that of natural abundance (93% in [7]Li-7% in [6]Li). In an enr-component, the isotopic enrichment in [6]Li is 95%.

can be easily done by acquiring quantitative data for each isotope. However, such an approach would require the use of an internal lithium reference inside the studied sample. This strategy is generally followed in liquid-state NMR. However, for solid materials, it appeared worthwhile to develop a method, without an internal reference, to quantify [7]Li and [6]Li using high resolution solid-state NMR techniques. It is the objective of this work.

The method we have developed was tested on several samples with unknown [7]Li/[6]Li isotope ratios. These samples consist of lithiated silicon-based electrodes in which isotopic enrichment was performed using an electrochemical method. The main [6]Li enrichment setups that were used in the present work are illustrated in Fig. 1.

To validate the methodology based on solid-state NMR, we also carried out the quantification using liquid state ^{7}Li and [6]Li NMR. On one hand, it should be easier to implement since internuclear and electron-to-nuclear interactions are averaged due to Brownian motion. On the other hand, the liquid-state [6,7]Li NMR requires a complete extraction and dissolution of lithium from electrode samples with a complete loss of information associated with different phases of the corresponding materials. Mass spectrometry analyses were also performed on the residue obtained from these solutions after drying to

22146 | *Phys. Chem. Chem. Phys.*, 2023, **25**, 22145–22154

This journal is © the Owner Societies 2023

determine the ^{7}Li/^{6}Li ratio and double cross-check the methodology we have proposed.

2. Results and discussion

2.1. Theoretical background and methodology development

From the experimental point of view, both ^{7}Li and ^{6}Li solid-state NMR can be easily carried out using classical probes dedicated to CPMAS experiments. The ^{6}Li nucleus, having a smaller gyromagnetic ratio and lower quadrupolar moment than ^{7}Li, usually results in better-resolved spectra. However, the low natural abundance of the ^{6}Li nucleus requires longer acquisition times for non-enriched samples. The main problem is to compare the integrals of ^{7}Li and ^{6}Li NMR signals. As a matter of fact, even if the measurements are performed on the same sample and the same NMR probe, at a given magnetic field (11.74 T in our case), the ^{7}Li and ^{6}Li NMR frequencies (Larmor frequencies) are 194.37 MHz and 73.6 MHz, respectively. This means that from an experimental point of view, the NMR probe has to be tuned and matched for each isotope in order to optimize the resonant circuit. It is known that such a circuit cannot deliver a linear response for a whole range of frequencies. Moreover the NMR signal is further filtered and amplified by electronic circuits. They are also not expected to have linear amplification in the whole NMR frequency range. These observations have been rationalized by different formulae describing the dependence on the signal-to-noise ratio, S/N, after a 90° pulse. Among the following options, one that has been very often used[23] and extensively discussed is outlined in the excellent review of Doty *et al.*[24]

$$\frac{S}{N} = \left[\frac{\bar{h}^2\sqrt{2\pi\mu_0}}{12k_b^{\frac{3}{2}}}\right]\left[\frac{n_s\gamma I_x(I_x+1)\sqrt{T_2^*}}{T_s\sqrt{T_n+T_p}}\right] \times (\eta_E\eta_f Q_L V_s)^{\frac{1}{2}}\omega^{\frac{3}{2}} \quad (1)$$

where $\bar{h}$ is Plank's constant divided by 2π, μ_0 is the permeability of free space, k_b is Boltzmann's constant, n_s is the number of spins at resonance per unit volume, γ is the gyromagnetic ratio, I_x is the spin quantum number, T_2^* is the effective spin–spin relaxation time, T_s is the sample temperature, T_n is the probe noise temperature, T_p is the effective preamp noise temperature, η_E is the RF efficiency, η_f is the filling factor of the resonant coil, Q_L is the quality factor of the matched circuit, V_s is the sample volume, and ω is the Larmor frequency, where $\omega = \gamma B_0$.[24]

The above equation eqn (1) shows that it is impossible to perform direct quantitative comparison of ^{7}Li and ^{6}Li without signal-to-noise (S/N) calibration for each isotope. However, it can be done with sufficient precision by using a reference compound with known isotope abundance and with similar physical properties (magnetic susceptibility, permittivity, *etc.*). After that, for any samples to be analyzed, provided that the measurements on each Li isotope are carried out under identical conditions, the calculated ^{7}Li$_{s/n}$ and ^{6}Li$_{s/n}$ ratios will depend only on the fraction of each isotope (n_s value in eqn (1)). Indeed, as ^{6}Li and ^{7}Li NMR experiments are performed on the same sample using the same spectrometer, then T_s, V_s,

B_0 and η_f are equivalent for both isotopes. For each isotope, γ and I_x, as well as h, μ_0 and k_B are constants. Moreover, due to the proximity of physical properties of the reference and studied samples, the Q_L and T_2^* factors also remain similar. Thus, the integral of measured NMR signals (int) of ^{6}Li and ^{7}Li will be, respectively, proportional to the amount (in %) of ^{6}Li and ^{7}Li nuclei:

$$\frac{\text{Int}(^7\text{Li})}{\text{Int}(^6\text{Li})} = S\frac{\%^7\text{Li}}{\%^6\text{Li}} \quad (2)$$

where S defines the normalization factor.

This relation allows calculating the isotopic ratio of any sample on the basis of the measured integrals. Note that the sum of %^{7}Li and %^{6}Li remains constant and is equal to 100%.

It is essential to remind that such a quantification is possible only if the acquisition conditions are optimized and kept constant: excitation pulse, acquisition delay (fulfilling a complete recovery of nuclear magnetization), tuning and matching of resonance circuit. Additionally, the number of scans (N) and the receiver gain (G) used to acquire NMR spectra with good quality can be easily taken into account: as a matter of fact, signal-to-noise ratios can be normalized by dividing the measured S/N ratio by G and N.[25,26] Note that the mass of the material does not need to be taken into account since the ^{7}Li and ^{6}Li measurements are performed in the same MAS rotor.

2.2. Determination of S factor and validation of the NMR method.

For the determination of the S factor, a powder of a lithiated silicon-based electrode was used as a reference. This silicon-based electrode was electrochemically lithiated using a Li metal counter electrode where lithium isotope abundance is around natural (92.7% in ^{7}Li–7.3% in ^{6}Li) in order to reach a lithiation state corresponding to 1000 mA h g^{-1} (related to active material).

Fig. 2 shows the ^{7}Li and ^{6}Li NMR spectra of the reference sample. The differences between ^{7}Li and ^{6}Li spectra are as expected. The signal-to-noise ratio for the ^{6}Li NMR spectrum is lower compared to the ^{7}Li NMR spectrum due to a lower gyromagnetic ratio and natural abundance of the ^{6}Li isotope. Moreover, the ^{7}Li NMR spectrum presents a spinning side band pattern (additional signals shifted by ν_{rot} relative to the isotropic lines). It is most likely due to the quadrupolar
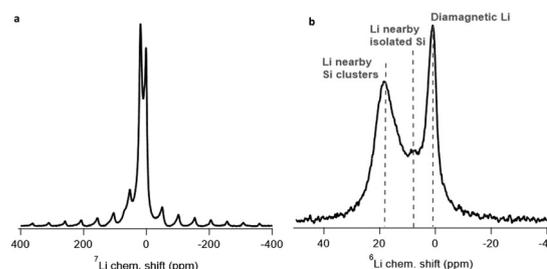

Fig. 2 ^{7}Li (a) and ^{6}Li (b) NMR spectra of the reference sample (lithiated silicon-based electrode with natural lithium isotopes abundance). The proposed assignments are based on ref. 16, 17 and 24.

interactions which are not averaged at the operating 10 kHz spinning rate. In contrast, for ^{6}Li, the quadrupolar moment is lower and almost no spinning side band is observed. These features can be overcome by increasing the spinning rate for ^{7}Li and/or by increasing the number of accumulated transients for ^{6}Li (or otherwise by increasing the magnetic field intensity).

Both ^{6}Li and ^{7}Li NMR spectra show the presence of several spectral components. The NMR signal with the chemical shift value of ~ 0 ppm is assigned usually to lithium atoms in the SEI. Two NMR lines near 19 and 6 ppm can be attributed to lithium in the Si bulk, namely to Li atoms nearby small Si clusters (stars, rings) and isolated Si, respectively. Indeed, similar signals were observed earlier for the stable alloys $Li_{12}Si_7$ and $Li_{15}Si_4$ with these characteristic local surroundings.[19,20] The first lithiation of crystalline Si is accompanied by the breaking of Si–Si bonds. This process requires high energy and leads to the so-called "core–shell" mechanism of lithiation with a shell made of an amorphous Li_xSi phase ($x = 2.8 \pm 0.3$), surrounding the core of pristine crystalline Si.[27,28] Taking it into account, it seems reasonable to associate the observed NMR signals near 19 and 6 ppm with Li atoms which are located in the bulk of the shell and with those found in the highly lithiated "core–shell" front, respectively.

It is of primary importance to check that the lithium isotope abundances in the sample and those in the counter electrode and electrolyte are alike. It has to be noted that there are some hypothetical phenomena, known as isotope fractionation, which could slightly modify this abundance leading to a small isotope enrichment of a component in one specific isotope. The preferential diffusion of one isotope over the other is an example of an isotope effect leading to isotope fractionation. Isotope fractionation generally leads to very small deviations from the natural ratio (parts per thousand)[1,29] and can be neglected. In reversible systems like Li-ion cells, there is no opportunity to observe kinetic fractionation; though equilibrium lithium fractionation could exist. On the other hand, some reactions during SEI formation can be irreversible and could cause a slight isotope fractionation at the electrode surface. In order to clarify this point, ToF-SIMS analyses were performed at the electrode surface where SEI is mainly present. Fig. 3 shows the ToF-SIMS profile obtained for the reference electrode. The evolution of the $^{30}Si^-$ fragment reflects that sputtering has been successful in probing the entire depth of the SEI and reaching the beginning of the bulk material as the $^{30}Si^-$ moiety reaches a plateau. ^{7}Li abundance measured is around 93% over the entire depth-profile. No isotope fractionation is observed. Thus, it can be concluded that ^{7}Li isotope abundance in this electrode is 93% and this sample can be used as a reference. Using the normalized integrals of ^{7}Li and ^{6}Li NMR signals, which are 3435 and 26, respectively, and using eqn (2), we calculate the correction factor S to be equal to about 10.5. Note that all the NMR lines shown in Fig. 2 were taken into account, including spinning side bands. In order to go a step further, the deconvolution of the measured NMR spectra has been performed.
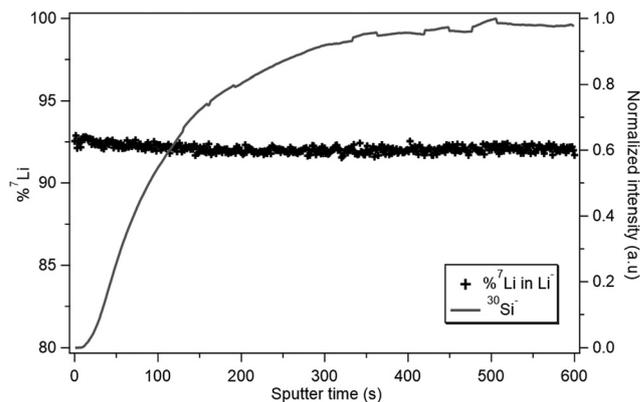

Fig. 3 ToF-SIMS profile of the silicon-based electrode used as a reference. The intensity of the $^{30}Si^-$ fragment (grey curve) is normalized by its maximum. The isotopic abundance in ^{7}Li (black dots) was measured due to $^6Li^-$ and $^7Li^-$ fragments.

As shown in Fig. 4, they can be considered as a superposition of three components: two "bulk" components, corresponding to lithium nearby isolated Si atoms ($Li_{15}Si_4$ in phase denomination) and lithium nearby Si clusters ($Li_{12}Si_7$), and Li atoms in the SEI with the characteristics presented in Table 1. It is clear from Table 1 that the proportions of each component (silicides and SEI) found in ^{7}Li and ^{6}Li NMR are alike within $\pm 3\%$, which reinforces the idea that there is no isotope fractionation detectable by NMR. In order to verify the consistency of the measurement performed, the lithiation of a silicon-
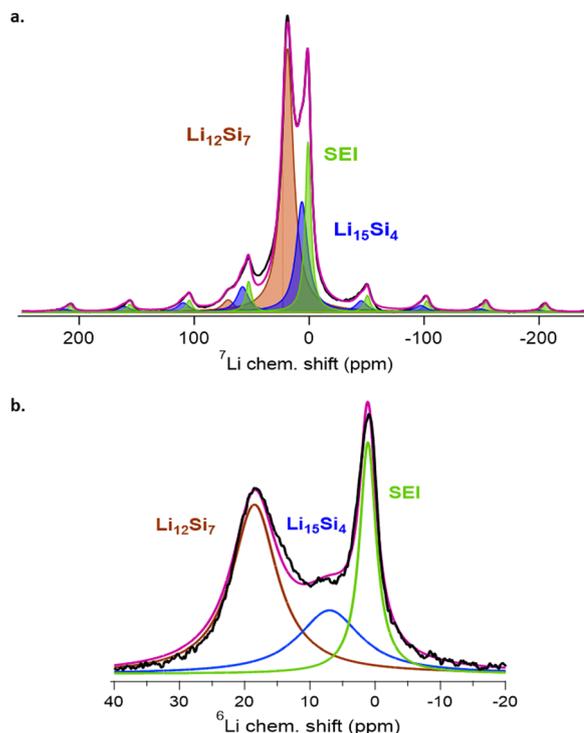

Fig. 4 ^{7}Li (a) and ^{6}Li (b) NMR spectra of the reference sample (lithiated silicon-based electrode with natural lithium isotopes abundances). The proposed assignments are based on ref. 19, 20, 31.

22148 | *Phys. Chem. Chem. Phys.*, 2023, **25**, 22145–22154

This journal is © the Owner Societies 2023

Table 1 Results and parameter simulations used for deconvolution with DMFit software[30]

	Line	Simulation parameters	δ (ppm)	Integral (%)	assignment
^{6}Li	#1	Gaus/Lor	18.83	44	$Li_{12}Si_7$
	#2	Gaus/Lor	6.31	34	$Li_{15}Si_4$
	#3	Gaus/Lor	0.99	22	SEI
^{7}Li	#1	Gaus/Lor + ssb	18.83	47	$Li_{12}Si_7$
	#2	Gaus/Lor + ssb	6.31	29	$Li_{15}Si_4$
	#3	Gaus/Lor + ssb	0.99	24	SEI

based electrode using a ^{6}Li (95%) metal counter electrode was carried out (Setup A). This simple experiment is the exact opposite of the one performed to get the reference sample. As previously mentioned, since isotopic fractionation is considered negligible, a value of 5% for the ^{7}Li content in the silicon electrode is expected and observed. Using the S factor, calculations give a value of 4% for ^{7}Li abundance. It clearly shows that the method we proposed can be applied for samples for which the isotopic ratio has to be determined. Let's note that here and further, different NMR signals are labeled and discussed as "phases": $Li_{12}Si_7$, Li_7Si_3, $Li_{13}Si_4$ and $Li_{15}Si_4$. However, it is done just for the sake of simplicity and we rather refer to their typical local lithium surroundings. It has to be also noted that at this stage of the discussion, we restricted ourselves to only two $Li_{12}Si_7$ and $Li_{15}Si_4$ "phases", which correspond to the lowest and the highest stages of silicon lithiation, respectively. However, a better fit of the spectra shown in Fig. 4 can be achieved if we include additional lines near 16 and 12 ppm. These signals correspond to lithium atoms with local coordinations consisting of Si dumbbells, and Si pairs and isolated atoms, respectively. They correspond to the "intermediary" Li_7Si_3 and $Li_{13}Si_4$ phases if one use the above denomination.[19,20] For further discussion (see below), we will use a larger set of lines during NMR spectra deconvolution.

2.3. Determination of the isotopic ratio on representative silicon-based electrode samples

In order to illustrate the reliability of the proposed methodology, three representative samples (B, C, D) obtained from experimental setups B, C and D, respectively, have been analyzed *ex situ*. These setups, as detailed in Fig. 1 and in the Experimental section, lead to different ^{6}Li-enrichment of the electrode components. Moreover, for these three samples, Li was also extracted in a liquid phase from the solid material according to the protocol described in the Experimental section. Liquid-state NMR analyses were performed to determine the isotopic abundances. After liquid-state NMR analyses, the solutions were also deposited on a silicon substrate to determine the isotopic abundances *via* ToF-SIMS. These two latter experiments were carried out to crosscheck the results obtained with solid-state MAS NMR.

Table 2 gathers the values of ^{7}Li enrichment measured by solid-state MAS NMR, liquid NMR and ToF-SIMS. The results obtained by using the three methods are fairly similar, with a variation of 1%.

Table 2 Percentages of ^{7}Li measured for the three samples #B, #C and #D using solid-state MAS NMR, liquid NMR and ToF-SIMS

	#B	#C	#D
^{7}Li measured by ss-NMR	88%	11%	74%
^{7}Li measured by liquid-NMR	88%	12%	74%
^{7}Li measured by ToF-SIMS	88%	13%	73%

2.4. Inputs of Li NMR tracing to study the Li dynamic in battery materials

Many tracing experiments are conceivable: the labelling of different cell components (cathode, anode and electrolyte) and of the components that are expected to be formed during cycling, such as the SEI. Experiments described in experimental setups B, C and D are some examples. In this section, we would like to focus on the study of Li exchange between electrolyte, SEI and Si core particles using isotope tracing and NMR characterization. Li exchange occurring between the SEI and the electrolyte has been first shown in a SEI-model generated on a copper foil through ToF-SIMS experiments conducted by Peng Lu *et al.*[2] Peng Lu and coworkers have interpreted their results as a permeation of the electrolyte in the first nanometers of the SEI combined with isotope exchanges in depth. From these results, the authors could infer the Li diffusion mechanisms in the SEI in their model setup. Beyond this aspect, this finding is important since it suggests that Li isotope exchange can take place between the liquid and solid media even when the system is at equilibrium, *i.e.* without any electrical potential. Our recent results also demonstrated that Li isotope exchanges can occur between the SEI of a delithiated graphite electrode and an electrolyte without any electric field.[10] Such exchanges are fast and have a large amplitude as isotope distribution becomes homogeneous in less than 20 minutes of contact. In both studies, the methodology is the same: a nat-SEI is dipping in an enr-electrolyte. Note that ToF-SIMS allows the evolution of the ^{7}Li/^{6}Li ratio on the surface of the electrode.

Our NMR technique is an efficient tool for studying homogeneous samples arranged in successive layers, such as a SEI film on substrate or delithiated graphite electrodes. However, the studied Si electrodes are not layered but rather porous materials, and the SEI can be found not only on the electrodes surfaces but also within their thickness. In this regard, NMR can be considered as a more powerful technique since it is able to investigate the whole sample volume.

To answer these addressed questions, a silicon-based electrode was lithiated against a Li metal counter electrode, where lithium isotope abundance was around natural (92.6% in ^{7}Li–7.4% in ^{6}Li) to a state of charge corresponding to 1000 mA h g^{-1}. The silicon electrode was then recovered and dipped into a ^{6}Li-enriched electrolyte (95% in ^{6}Li) for 52 hours. These procedures correspond to experimental setup D (Fig. 1D). Fig. 5 shows the ^{7}Li (a) and ^{6}Li (b) NMR spectra of electrode powder at the end of the experiment. The results of spectra deconvolution are present in Table S1 in the ESI.† The corresponding isotopic ratios are reported in Table 3. As can be seen
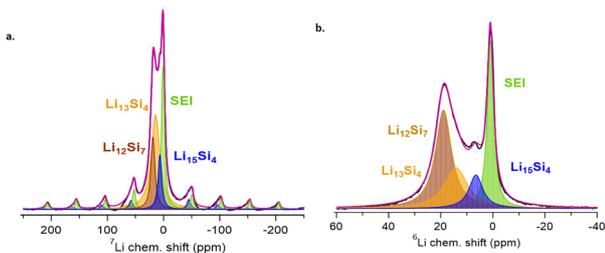
This journal is © the Owner Societies 2023

Phys. Chem. Chem. Phys., 2023, **25**, 22145–22154 | **22149**

Fig. 5 ^{7}Li (a) and ^{6}Li (b) NMR spectra of the reference electrode dipped into a ^{6}Li-electrolyte. The proposed NMR signal assignments are based on ref. 16, 17, 28.

from NMR data, for all Li$_{x}$Si phases and SEI, the ^{7}Li abundance deviates from the natural one (Table 3). This confirms that silicide particles are also affected by the isotope exchange phenomenon, and its extent is high enough to be observed by NMR. The mean ^{7}Li abundance determined using our methodology is 74%. This value is close to that obtained from electrochemical results (see the ESI,† calculation used for mass balance), yielding a ^{7}Li concentration of 71% for the complete system, electrolyte + electrode, with the homogenization of a full isotope.

However, the distribution of lithium isotopes in different phases is highly non-uniform: meanwhile for the SEI, Li$_{13}$Si$_{4}$ and Li$_{15}$Si$_{4}$ exhibit a ^{7}Li abundance of around 80 ± 3%, while for Li$_{12}$Si$_{7}$, it does not exceed 50% (*i.e.* it is the most enriched in ^{6}Li). The observation of ^{6}Li fractionation in different Li$_{x}$Si silicides can be explained if we assume again that the lithium concentration increases with the shell depth: on the Si grain boundary, the Li environment is similar to that in the poorly lithiated Li$_{12}$Si$_{7}$, while for the deepest "core–shell" front, it is rather reminiscent of that for Li$_{15}$Si$_{4}$ (while the "intermediary" phase Li$_{13}$Si$_{4}$ corresponds obviously to Li atoms in the shell depth). In this case, the difference in ^{6}Li enrichment between different Li$_{x}$Si silicides can be determined by different lithium mobility in these phases. For instance, Dupke *et al.*[8] have shown that lithium ions interacting with silicon clusters or dimers have generally higher mobilities than those surrounded by monomeric silicon atoms. Consequently, Li mobility becomes more and more limited according to the order: Li$_{12}$Si$_{7}$ → Li$_{7}$Si$_{3}$ → Li$_{13}$Si$_{4}$ → Li$_{15}$Si$_{4}$.[19]

At first sight, the most intriguing finding is the high fraction of ^{7}Li in the SEI. Considering that the SEI covers the silicon surface, the ^{6}Li atoms must pass through this domain to reach the Si depth. From this point of view, one would expect a higher fraction of ^{6}Li in the SEI. However, two phenomena have to be taken into account. The first one concerns lithium mobility.

Lithium diffusion coefficients are, respectively, estimated to be around 1.6×10^{-16} cm^{2} s^{-1} for Li$_{2}$O; 3.5×10^{-16} cm^{2} s^{-1} for LiF; 1.1×10^{-11} cm^{2} s^{-1} for ROLi and 7×10^{-12} cm^{2} s^{-1} for ROCO2Li[31,32] which are typical compounds found in the SEI,[33] whereas the lithium diffusion coefficient in silicon is estimated to be 10^{-11} cm^{2} s^{-1}.[28,34,35] The second aspect to consider is that not all the silicon surface can be covered with the SEI. Indeed, the states of Si powder in electrochemical cycling (pressed and stuck to copper foil) and in our experiment (free powder dipped in a liquid electrolyte) are significantly different. In our case, new regions of the Si surface, previously inaccessible for direct contact with the electrolyte, may open up. Thus, the diffusion of ^{6}Li in the Si depth can occur directly across the silicides grains bypassing the SEI.

In order to better understand the processes involved in lithium isotope exchange, an "*in situ*" MAS NMR experiment was performed. For this, a few drops of a ^{6}Li-electrolyte were added in a rotor filled with a ^{7}Li-lithiathed electrode. Then, the NMR measurements were performed after only one hour of contact. NMR spectra, which correspond to 48 accumulated transients with a 4 s recycling delay, were acquired continuously with a 900 s delay between each spectrum. Fig. 6 displays the ^{7}Li NMR spectra obtained during the sequential acquisition process.

Fig. 7 shows the deconvolution of ^{7}Li MAS NMR spectra focusing solely on the central transition (the ssb parameters have been taken into account but are not shown in the figure for clarity). Fig. 8 presents the evolution of ^{7}Li signal intensities (see Table S2, ESI†) in different phases as a function of the soaking time with the ^{6}Li 95% enriched electrolyte.

It is clear from these experimental data that the fractions of ^{7}Li in the electrolyte do not vary significantly over time. If we consider the electrolyte as the only reservoir of ^{6}Li, then the corresponding NMR signal should be the first to be modified if isotope exchanges take place. Therefore, we have to conclude that either the lithium isotope exchanges involving the liquid electrolyte and solid powder do not occur, or they have already taken place during the first non-monitored hour. To check it, the Tof-SIMS experiments have been performed. These data (see Fig. 9) clearly demonstrate that the "liquid–solid" isotope
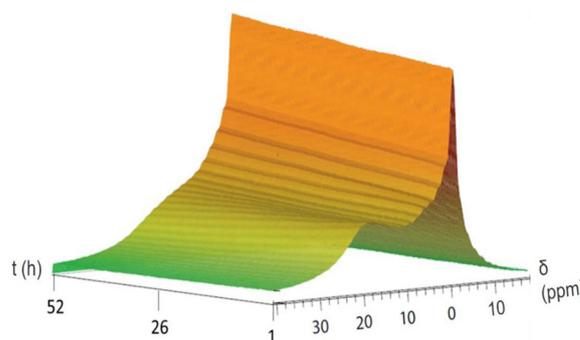

Fig. 6 Evolution of the ^{7}Li distribution in a soaking experiment between a ^{6}Li 95%-enriched electrolyte and a lithiated silicon-based electrode. ^{7}Li-NMR spectra (48 accumulated transients).
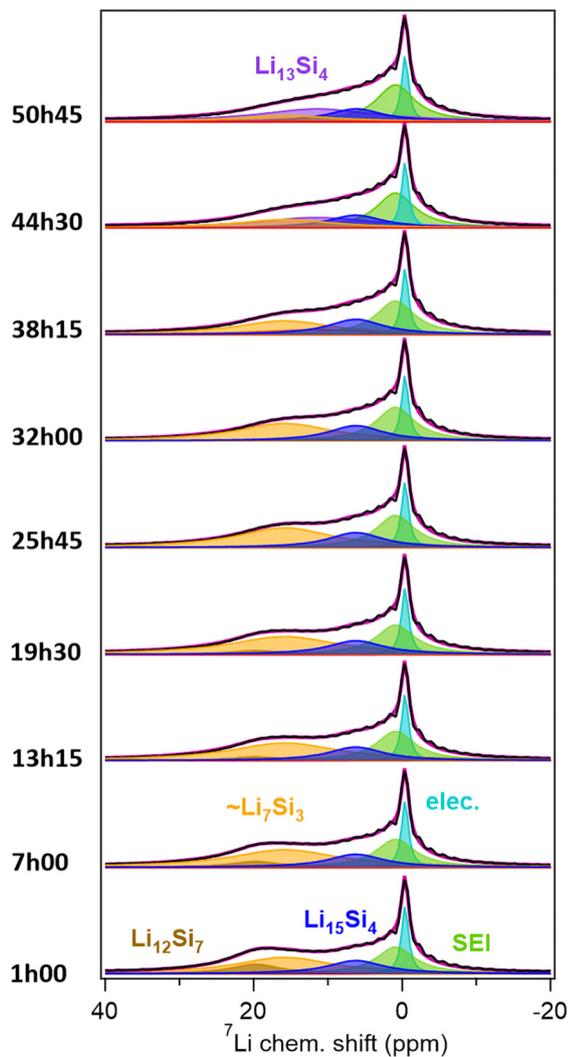
Table 3 Isotopic abundance in ^{7}Li determined by solid state NMR

Assignment	Isotopic abundance in ^{7}Li (%)
SEI	78
Li$_{12}$Si$_{7}$	49
Li$_{13}$Si$_{4}$	83
Li$_{15}$Si$_{4}$	78

22150 | *Phys. Chem. Chem. Phys.*, 2023, **25**, 22145–22154

This journal is © the Owner Societies 2023

Fig. 7 Soaking experiment between a ^{6}Li 95%-enriched electrolyte and a ^{7}Li lithiated silicon-based electrode. Deconvolution of ^{7}Li MAS NMR spectra after 1 h, 7 h, 13 h 15 min, 19 h 30 min, 25 h 45 min, 32 h, 38 h 15 min, 44 h 30 min, and 50 h 45 min of soaking time.

Fig. 8 Evolution of the ^{7}Li distribution in a soaking experiment between a ^{6}Li 95%-enriched electrolyte and a lithiated silicon-based electrode. The solid lines are added as the guides for eyes.

Fig. 9 Percentage of the ^{7}Li isotope measured *via* ToF-SIMS in the electrode as a function of soaking time with the ^{6}Li-based electrolyte. The values were obtained by sputtering the samples in the ToF-SIMS instrument during 0 s, 50 s, 150 s, 200 s, and 250 s.

exchange is completely finished during the first hour of soaking. The percentage of ^{7}Li decreases sharply from 93% to 55% during the first ten minutes over the entire depth probed, reflecting a diffusion of ^{6}Li atoms at the surface of the electrode. Curiously, after 30 minutes of immersion, the percentage of ^{7}Li rises to around 75% in the probed depth and to 65% at the surface (0 s of sputtering). Finally, after 60 minutes of immersion, the percentage of ^{7}Li is around 75% for the entire depth probed. This can be explained by mutual ^{6,7}Li diffusion, when ^{6}Li atoms penetrate to deeper Si layers, while ^{7}Li diffuses from the Si depth to the surface, until reaching the homogenized concentration.

The main changes in the ^{7}Li fraction are found on the silicides surface: during 25 hours, the ^{7}Li$_{12}$Si$_7$ phase completely disappears (Fig. 6–8), most likely due to the ^{6}Li → ^{7}Li replacement. This confirms our previous results and assumptions (see Fig. 5 and corresponding discussion). Interestingly, the

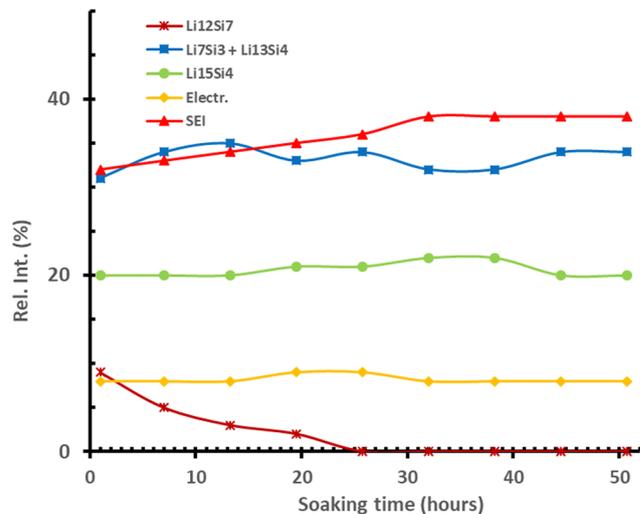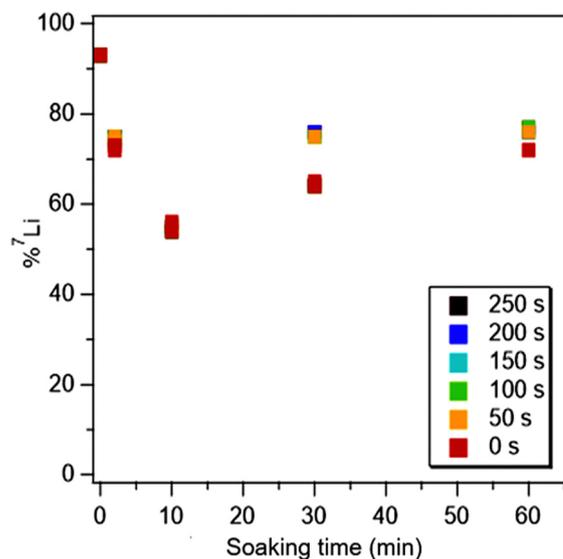decrease in ^{7}Li$_{12}$Si$_7$ phase intensity is accompanied by an increase in the ^{7}Li fraction in the SEI, from about 32 to 38%. As in the case of ToF-SIMS data, this result allows assuming that besides ^{6}Li → ^{7}Li replacement, there is a simultaneous inverse process of ^{7}Li → ^{6}Li occurring between silicides and SEI compounds. It has to be noted also that in contrast to the outer part of the Li$_x$Si shell, the behavior of ^{7}Li fraction in deeper layers remains almost unchanged with soaking time. For the "core–shell" interface (which is represented as the Li$_{15}$Si$_4$ phase as shown in Fig. 8), it seems to be obvious. For the intermediary part of the shell, the situation is more

This journal is © the Owner Societies 2023

Phys. Chem. Chem. Phys., 2023, **25**, 22145–22154 | **22151**

complicated. Fig. 7 presents one of the possible fits with two NMR lines corresponding to Li_7Si_3 and $Li_{13}Si_4$ phases. Within this representation with two separate "intermediary" lines, the tendency to decrease the Li_7Si_3 phase amount is observed. Thus, ^6Li penetration is observed in these layers of the Li_xSi shell. However, it has to be noted that the fit of NMR spectra in the range of chemical shifts around 15 ppm yields rather contradictory results. Due to their proximity, these NMR lines overlap each other. As a result, their parameters (shift, width, ssb distribution) can be changed in a substantially wide range and, consequently, their intensities also change within the large error bars. Therefore, it appears to be more reasonable to represent them as a whole "Li_7Si_3 + $Li_{13}Si_4$" phase (as shown in Fig. 8 and in Table S2, ESI†). Then it becomes clear that the ^7Li fraction remains stable (within ±2% of relative intensity) during entire soaking time. The center of mass of this merged NMR line moves in the region of lower chemical shifts, indicating, most likely, the ^7Li atoms' diffusion in the deeper layers of the Li_xSi shell.

Thus, we can propose the "two-stage" scenario of the ^6Li–^7Li isotope exchange in the ^6Li-enriched liquid electrolyte–^7Li lithiated Si electrode system. During the first 30 min, the fast "liquid–solid" exchange occurs, involving, most likely, both the silicide surface and the SEI. Then the ^6Li atoms start to permeate Si bulk, replacing the ^7Li ones, which in turn sink deeper in Si particles and/or diffuse in the SEI. This exchange process is much slower (occurs on the scale of tens of hours) and is most likely limited to only the outer part of the Li_xSi shell.

3. Conclusions

A simple and easy-to-use methodology of lithium isotope titration by high-resolution magic angle spinning solid-state NMR has been proposed. A key point is the use of a reference sample that allows comparing ^7Li and ^6Li MAS NMR spectra for all acquisitions under the same conditions without the distortion of spectra. The spectra deconvolution makes it possible to determine the isotopes' ratio for each local chemical environment of the nucleus-probe. Therefore, in silicon-based electrode samples, it was possible to quantify $^7Li/^6Li$ for the SEI, electrolyte and different silicides.

In the second step, this method was applied to study the isotope exchanges appearing between a ^7Li–Si electrode in a partially lithiated state (1000 mA h g^{-1}) and a ^6Li-enriched electrolyte. The NMR results in combination with ToF-SIMS data demonstrate that Li isotope exchanges occur most likely due to a "two-stage" mechanism. During the first hour of the electrode and electrolyte contact, the fast "liquid–solid" ^6Li–^7Li exchange occurs, involving both the SEI and silicide surface. Then, these ^6Li atoms start to permeate into the Si bulk, replacing the ^7Li ones. This process is much slower and occurs on a scale of tens of hours.

It is worth noting that although in the present work we have considered the battery electrode materials as an example to illustrate our methodological approach, it can be applied in a wide range of systems, for example, to study the chemical reactions involving atomic exchanges such as those expected between different solid phases or in liquid–solid reactions. The method proposed can be performed on standard MAS NMR equipment without involving any additional techniques.

4. Experimental

4.1. Electrochemistry

Silicon based electrodes were prepared by mixing 70 wt% of silicon nanoparticles, 15 wt% of binder (PAA), 10% of carbon black (Super P) and 5% of carbon fibers (VGCF) in aqueous solution. The classical procedures of coating, drying and compressing resulted in an active material loading of 3.80 mg cm^{-2} on a copper foil (10 μm).

Electrolytes were prepared in a glovebox by dissolving the $LiPF_6$ salt in the ethylene carbonate/dimethylcarbonate (EC/DMC 1/1 wt) mixture containing 10 wt% of fluoroethylene carbonate in order to obtain a concentration of 1 mol L^{-1}. Electrolytes were achieved in small amounts to avoid any degradation of the solution over time. For the ^6Li-enriched electrolyte, a $^6LiPF_6$ enriched at 95% (Sigma-Aldrich) was used.

Si//Li half-cells were assembled in a pouch cell by stacking the silicon-based electrode (35 × 35 mm), a separator (Celgard 2400, 40 mm × 40 mm) and a foil of lithium metal deposited on copper. The ^6Li metal foil was obtained by flattening chunks enriched at 95% in ^6Li. A volume of 150 μL of electrolyte was deposited on the separator, and then the cells were sealed in an argon filled glovebox.

Galvanostatic cycling was carried out in a battery tester (Arbin) with a current of 1.3 mA until reaching a specific capacity of 1000 mA h g^{-1} during the discharge. The cut-off potentials were limited to 10 mV and 1.2 V. If the galvanostatic cycling failed to reach the targeted capacity, a floating step was carried out at 10 mV. At the end of cycling, the cells were disassembled in an argon filled glovebox. Silicon-based electrodes were taken off and washed by soaking in DMC during 1 minute. One part of the electrode was kept for solid-state NMR and the other used for ToF-SIMS and liquid-NMR characterizations.

4.2. Sample preparation

A powder obtained from a lithiated silicon-based electrode was used as a standard for the development of the methodology. In this sample, lithium isotopes are present in natural abundance. The electrode samples on which the validity of the methodology was tested were enriched in ^6Li electrochemically. Four kinds of enrichment were carried out by introducing ^6Li in different parts of the accumulator. The preparation conditions of the four samples are summarized in Fig. 1. To make reading easier, terms "nat" and "enr" are used to characterize respectively "natural" and "enriched" components in ^6Li. In a nat-component, the lithium isotopic ratio is that of natural

22152 | *Phys. Chem. Chem. Phys.*, 2023, **25**, 22145–22154

This journal is © the Owner Societies 2023

abundance *i.e.* ~93% in ^{7}Li. In an enr-component, the isotopic enrichment in ^{6}Li is 95%.

4.3. Solid-state NMR characterizations

^{7}Li and ^{6}Li NMR spectra have been obtained at 194.37 MHz and 73.6 MHz, respectively, on a Bruker AVANCE III 500 MHz spectrometer equipped with a 4 mm Bruker CPMAS probehead. Tuning of the probe has to be carried out when changing the observed nucleus. The Magic Angle Spinning method is used by setting the spinning rate at 10 kHz. The acquisition sequence used is direct excitation without proton decoupling using a 30° pulse, 2.5 µs and 2 µs for ^{6}Li and ^{7}Li, respectively. Dead times were set to 40 µs and 0.4 µs and recycling delays to 5.6 s and 0.66 s for ^{6}Li and ^{7}Li, respectively. At first sight, these recycling delays may appear to be too short. Indeed, rough estimates showed that in Li_xSi phases, the spin–lattice relaxation time, T_1, for the ^{7}Li nuclei was in the range of about 0.4 s which is close to the values obtained by Kuhn *et al.*[36] Thus, the recycling delay of 0.66 s is much shorter than the "classical" required $5T_1$. It has to be noted, however, that we deliberately choose the shortest possible value of repetition time in order to maximize the number of FID accumulations. We made sure that the shape of the ^{6}Li and ^{7}Li NMR spectra at given delays does not differ significantly from that obtained at longer repetition times. Other parameters such as the number of accumulated transients (NS) and receiver gain (RG) have to be taken into account for quantitative treatment (see the Results section).

4.4. Liquid NMR characterizations

In order to carry out liquid state NMR analyses, cells were first disassembled in a glovebox. After separation of components, electrodes were washed by soaking in DMC during 1 min. Then they were scratched in order to separate the copper collector from the rest of the electrode. The powder obtained is placed in a crucible in nickel in which one or two tablets of sodium hydroxide (Sigma Aldrich®) are added. Then, the crucible is heated until everything is melted. Few drops of MilliQ® water are added in order to dissolve the solution of sodium hydroxide.

^{7}Li NMR and ^{6}Li NMR spectra were obtained, respectively, at 194.37 MHz and 73.6 MHz on the same Bruker AVANCE III 500 MHz spectrometer as for solid-state NMR. An electrolyte consisting of a mixture of EC:PC:DMC + 2% VC (1 M LiPF$_6$) was used to calibrate the ^{6}Li and ^{7}Li ratios, in the same manner as for the solid sample. The one pulse acquisition was used. In this sample, NMR spectra were acquired on a Bruker BBI 5 mm probe. For this sample recycling, delays of 1.23 s and 68 s were used for ^{7}Li and ^{6}Li NMR, respectively. For standard conditions, the number of accumulated transients was typically 128 with recycling delays of 1.23 s and 68 s for ^{7}Li and ^{6}Li, respectively.

4.5. ToF-SIMS characterizations

Few drops of solution were deposited on a silicon wafer and heated in an oven at 50 °C during about 15 minutes. ToF-SIMS analyses were achieved on a ToF-SIMS^5 ION-TOF spectrometer by using a Bi$_1^+$ beam at 15 keV. For each wafer, three acquisitions were carried out in a positive mode on a 150 × 150 µm^2 area.

Author contributions

The manuscript was written through contributions of all authors. All authors have given approval to the final version of the manuscript.

Conflicts of interest

There are no conflicts of interest to declare.

Acknowledgements

Notes and references

1 M. Tiwari, A. K. Singh and D. K. Sinha, *Chemostratigraphy*, Elsevier, 2015, pp. 65–92.

2 P. Lu and S. J. Harris, Lithium transport within the solid electrolyte interphase, *Electrochem. Commun.*, 2011, **13**, 1035–1037.

3 Z. Liu, P. Lu, Q. Zhang, X. Xiao, Y. Qi and L.-Q. Chen, A Bottom-Up Formation Mechanism of Solid Electrolyte Interphase Revealed by Isotope-Assisted Time-of-Flight Secondary Ion Mass Spectrometry, *J. Phys. Chem. Lett.*, 2018, **9**, 5508–5514.

4 S. Shi, P. Lu, Z. Liu, Y. Qi, L. G. Hector, H. Li and S. J. Harris, Direct Calculation of Li-Ion Transport in the Solid Electrolyte Interphase, *J. Am. Chem. Soc.*, 2012, **134**, 15476–15487.

5 N. Kuwata, M. Nakane, T. Miyazaki, K. Mitsuishi and J. Kawamura, Lithium diffusion coefficient in LiMn$_2$O$_4$ thin films measured by secondary ion mass spectrometry with ion-exchange method, *Solid State Ionics*, 2018, **320**, 266–271.

6 N. Kuwata, X. Lu, T. Miyazaki, Y. Iwai, T. Tanabe and J. Kawamura, Lithium diffusion coefficient in amorphous lithium phosphate thin films measured by secondary ion mass spectrometry with isotope exchange methods, *Solid State Ionics*, 2016, **294**, 59–66.

7 J. Zheng, M. Tang and Y. Hu, Lithium Ion Pathway within Li$_7$La$_3$Zr$_2$O$_{12}$-Polyethylene Oxide Composite Electrolytes, *Angew. Chem., Int. Ed.*, 2016, **55**, 12538–12542.

8 S. Dupke, T. Langer, F. Winter, R. Pöttgen, M. Winter and H. Eckert, Ionic Pathways in Li$_{13}$Si$_4$ investigated by ^{6}Li and ^{7}Li solid state NMR experiments, *Solid State Nucl. Magn. Reson.*, 2015, **65**, 99–106.

This journal is © the Owner Societies 2023

Phys. Chem. Chem. Phys., 2023, **25**, 22145–22154 | 22153

9 E. Hüger, L. Dörrer and H. Schmidt, Permeation, Solubility, Diffusion and Segregation of Lithium in Amorphous Silicon Layers, *Chem. Mater.*, 2018, **30**, 3254–3264.

10 M. Berthault, J. Santos-Peña, D. Lemordant and E. D. Vito, Dynamics of the $^6Li/^7Li$ Exchange at a Graphite–Solid Electrolyte Interphase: A Time of Flight–Secondary Ion Mass Spectrometry Study, *J. Phys. Chem. C*, 2021, **125**, 6026–6033.

11 A. L. Michan, M. Leskes and C. P. Grey, Voltage Dependent Solid Electrolyte Interphase Formation in Silicon Electrodes: Monitoring the Formation of Organic Decomposition Products, *Chem. Mater.*, 2016, **28**, 385–398.

12 N. Kuwata, G. Hasegawa, D. Maeda, N. Ishigaki, T. Miyazaki and J. Kawamura, Tracer Diffusion Coefficients of Li Ions in $Li_xMn_2O_4$ Thin Films Observed by Isotope Exchange Secondary Ion Mass Spectrometry, *J. Phys. Chem. C*, 2020, **124**, 22981–22992.

13 G. Hasegawa, N. Kuwata, Y. Tanaka, T. Miyazaki, N. Ishigaki, K. Takada and J. Kawamura, Tracer diffusion coefficients of Li^+ ions in *c*-axis oriented Li_xCoO_2 thin films measured by secondary ion mass spectrometry, *Phys. Chem. Chem. Phys.*, 2021, **23**, 2438–2448.

14 M. Diehl, M. Evertz, M. Winter and S. Nowak, Deciphering the lithium ion movement in lithium ion batteries: determination of the isotopic abundances of ^6Li and ^7Li, *RSC Adv.*, 2019, **9**, 12055–12062.

15 A. J. Ilott and A. Jerschow, Probing Solid-Electrolyte Interphase (SEI) Growth and Ion Permeability at Undriven Electrolyte–Metal Interfaces Using ^7Li NMR, *J. Phys. Chem. C*, 2018, **122**, 12598–12604.

16 M. Murakami, S. Shimizu, Y. Noda, K. Takegoshi, H. Arai, Y. Uchimoto and Z. Ogumi, Spontaneous Lithium Transportation via $LiMn_2O_4$/Electrolyte Interface Studied by $^{6/7}Li$ Solid-State Nuclear Magnetic Resonance, *Electrochim. Acta*, 2014, **147**, 540–544.

17 A. B. Gunnarsdóttir, S. Vema, S. Menkin, L. E. Marbella and C. P. Grey, Investigating the effect of a fluoroethylene carbonate additive on lithium deposition and the solid electrolyte interphase in lithium metal batteries using *in situ* NMR spectroscopy, *J. Mater. Chem. A*, 2020, **8**, 14975–14992.

18 T. Kobayashi, T. Ohnishi, T. Osawa, A. Pratt, S. Tear, S. Shimoda, H. Baba, M. Laitinen and T. Sajavaara, In-Operando Lithium-Ion Transport Tracking in an All-Solid-State Battery, *Small*, 2022, **18**, 2204455.

19 S. Dupke, T. Langer, R. Pöttgen, M. Winter, S. Passerini and H. Eckert, Structural characterization of the lithium silicides $Li_{15}Si_4$, $Li_{13}Si_4$, and Li_7Si_3 using solid state NMR, *Phys. Chem. Chem. Phys.*, 2012, **14**, 6496.

20 B. Key, R. Bhattacharyya, M. Morcrette, V. Seznéc, J.-M. Tarascon and C. P. Grey, Real-Time NMR Investigations of Structural Changes in Silicon Electrodes for Lithium-Ion Batteries, *J. Am. Chem. Soc.*, 2009, **131**, 9239–9249.

21 R. E. Gerald, C. S. Johnson, J. W. Rathke, R. J. Klingler, G. Sandí and L. G. Scanlon, ^7Li NMR study of intercalated lithium in curved carbon lattices, *J. Power Sources*, 2000, **89**, 237–243.

22 H. J. Chang, N. M. Trease, A. J. Ilott, D. Zeng, L.-S. Du, A. Jerschow and C. P. Grey, Investigating Li Microstructure Formation on Li Anodes for Lithium Batteries by in Situ $^6Li/^7Li$ NMR and SEM, *J. Phys. Chem. C*, 2015, **119**, 16443–16451.

23 D. I. Hoult and N. S. Ginsberg, The Quantum Origins of the Free Induction Decay Signal and Spin Noise, *J. Magn. Reson.*, 2001, **148**, 182–199.

24 F. D. Doty, G. Entzminger, J. Kulkarni, K. Pamarthy and J. P. Staab, Radio frequency coil technology for small-animal MRI, *NMR Biomed.*, 2007, **20**, 304–325.

25 H. Mo, J. S. Harwood and D. Raftery, A quick diagnostic test for NMR receiver gain compression, *Magn. Reson. Chem.*, 2010, **48**, 782–786.

26 H. Mo, J. S. Harwood and D. Raftery, Receiver gain function: the actual NMR receiver gain: receiver gain function, *Magn. Reson. Chem.*, 2010, **48**, 235–238.

27 E. Radvanyi, E. De Vito, W. Porcher, J. Danet, P. Desbois, J.-F. Colin and S. J. Si Larbi, Study of lithiation mechanisms in silicon electrodes by Auger Electron Spectroscopy, *J. Mater. Chem. A*, 2013, **1**, 4956.

28 J. W. Wang, Y. He, F. Fan, X. H. Liu, S. Xia, Y. Liu, C. T. Harris, H. Li, J. Y. Huang, S. X. Mao and T. Zhu, Two-Phase Electrochemical Lithiation in Amorphous Silicon, *Nano Lett.*, 2013, **13**, 709–715.

29 E. A. Schauble, Applying Stable Isotope Fractionation Theory to New Systems, *Rev. Mineral. Geochem.*, 2004, **55**, 65–111.

30 D. Massiot, F. Fayon, M. Capron, I. King, S. Le Calvé, B. Alonso, J.-O. Durand, B. Bujoli, Z. Gan and G. Hoatson, Modelling one- and two-dimensional solid-state NMR spectra: modelling 1D and 2D solid-state NMR spectra, *Magn. Reson. Chem.*, 2002, **40**, 70–76.

31 P. Guan, L. Liu and X. Lin, Simulation and Experiment on Solid Electrolyte Interphase (SEI) Morphology Evolution and Lithium-Ion Diffusion, *J. Electrochem. Soc.*, 2015, **162**, A1798–A1808.

32 M. B. Pinson and M. Z. Bazant, Theory of SEI Formation in Rechargeable Batteries: Capacity Fade, Accelerated Aging and Lifetime Prediction, *J. Electrochem. Soc.*, 2013, **160**, A243–A250.

33 P. Verma, P. Maire and P. Novák, A review of the features and analyses of the solid electrolyte interphase in Li-ion batteries, *Electrochim. Acta*, 2010, **55**, 6332–6341.

34 N. Ding, J. Xu, Y. X. Yao, G. Wegner, X. Fang, C. H. Chen and I. Lieberwirth, Determination of the diffusion coefficient of lithium ions in nano-Si, *Solid State Ionics*, 2009, **180**, 222–225.

35 G. A. Tritsaris, K. Zhao, O. U. Okeke and E. Kaxiras, Diffusion of Lithium in Bulk Amorphous Silicon: A Theoretical Study, *J. Phys. Chem. C*, 2012, **116**, 22212–22216.

36 A. Kuhn, P. Sreeraj, R. Pöttgen, H.-D. Wiemhöfer, M. Wilkening and P. Heitjans, Li Ion Diffusion in the Anode Material $Li_{12}Si_7$: Ultrafast Quasi-1D Diffusion and Two Distinct Fast 3D Jump Processes Separately Revealed by 7 Li NMR Relaxometry, *J. Am. Chem. Soc.*, 2011, **133**(29), 11018–11021.

22154 | *Phys. Chem. Chem. Phys.*, 2023, **25**, 22145–22154

This journal is © the Owner Societies 2023